High spin spectroscopy in ^{34}Cl

Abhijit Bisoi,[1] M. Saha Sarkar,[1,*] S. Sarkar,[2] S. Ray,[1] D. Pramanik,[2] R. Kshetri,[1,†] Somnath Nag,[3] K. Selvakumar,[3] P. Singh,[3] A. Goswami,[1] S. Saha,[4] J. Sethi,[4] T. Trivedi,[4] B. S. Naidu,[4] R. Donthi,[4] V. Nanal,[4] and R. Palit[4]

[1]*Saha Institute of Nuclear Physics, Bidhannagar, Kolkata 700064, India*
[2]*Bengal Engineering and Science University, Shibpur, Howrah 711103, India*
[3]*Indian Institute of Technology, Kharagpur 721302, India*
[4]*Tata Institute of Fundamental Research, Mumbai 400005, India*

(Received 29 November 2013; published 5 February 2014)

High spin states of ^{34}Cl populated through ^{27}Al(^{12}C,αn)^{34}Cl reaction at $E(^{12}\text{C}) = 40$ MeV, have been studied using the Indian National Gamma Array facility. The level scheme has been extended up to 10.6 MeV utilizing the results of intensity, directional correlation, and linear polarization measurements. Lifetimes of a few excited states have been estimated for the first time using the Doppler shift attenuation method. Large-basis shell-model calculations within the sd-pf space have been done to understand the microscopic origin of the excited states. Involvement of pf orbitals have been found to be essential to reproduce the negative-parity as well as high spin positive-parity states. Onset of collectivity manifested through short half-lives and large $B(E2)$ values have been reproduced well in the calculations.

DOI: 10.1103/PhysRevC.89.024303 PACS number(s): 23.20.Lv, 21.10.Tg, 21.60.Cs, 27.30.+t

I. INTRODUCTION

Study of spectroscopic properties of upper sd shell nuclei provides important information about different distinctive features of nuclear structure like single-particle and collective modes of excitations and their interplay and α cluster structure and its correlation with the superdeformed states [1–3]. The low spin spectra of most of the nuclei in this mass region show a single-particle mode of excitation [4,5], which evolves in collectivity manifested through superdeformation in ^{35}Cl [1], ^{36}Ar [2], and ^{40}Ca [3] at higher spins. Thus, these nuclei give us a unique opportunity to study the competition and combination of these two modes of excitation both experimentally and theoretically. The experimental signature of enhanced collectivity is a regularity in the excitation spectra and very short level lifetimes. Theoretically, these collective states are well explained within the configuration of mixed large-scale shell models in sd-pf basis [1–3]. Measurements of energy spectra as well as level lifetimes are therefore important to understand the underlying structure of different states.

The low spin positive-parity energy levels of upper-sd shell nuclei have been fairly successfully explained using untruncated sd shell-model calculations [6]. However, for negative parity and higher spin positive-parity states, intruder configurations from the neighboring pf shell become relevant. Even after the availability of improved computational facilities, untruncated calculation involving full sd-pf shells is not feasible. The nuclei in the sd-pf interface are of considerable recent interest to study the effects of several options of truncation in this model space.

^{34}Cl is an odd-odd nucleus in the sd shell ($Z = N = 17$). The ground state of ^{34}Cl has a shorter half-life (0^+, 1.53 s) than the isomer (3^+, 32 m) located 146 keV above, which decays by β^+ emission to the excited states of ^{34}S. These properties of ^{34}Cl are similar to those of ^{26}Al [7] to some extent. However, in ^{26}Al, the ground state has higher spin (5^+) and longer half-life (0.72 My) than the isomer (0^+, 6.34 s) located 228 keV above, which decays to ^{26}Mg. The β decay of the isomer at 146 keV in ^{34}Cl followed by delayed γ transitions with characteristic energies has been suggested as possible nova observables. The isotopic abundance ratio of ^{32}S/^{33}S has been used as an indicator of presolar grains of nova origin [7]. However, this ratio is directly influenced by ^{33}S$(p,\gamma)^{34}$Cl reaction because it destroys the ^{33}S abundance in the novae. Therefore, more experimental information about the low-lying spectra of ^{34}Cl is needed for understanding the large ^{33}S abundance observed in nova.

This nucleus has been extensively studied [4] using proton and α beams but there are few experiments where heavy ions were used [8,9]. In the present work, heavy-ion beams are used to extend the spectroscopic data for high spin states especially above 5 MeV. Spin, parity, and the mixing ratios of several levels and transitions have been measured by directional correlation ratio and polarization measurement. We have also determined the lifetimes of a few short-lived states using the Doppler shift attenuation method (DSAM) to identify the deformed states at higher excitation energy. Large-basis shell-model (LBSM) calculations have been done to interpret the experimental data. Several options of truncation were adopted, which provided useful insight into the sd-pf cross-shell calculations.

II. EXPERIMENTAL DETAILS AND DATA ANALYSIS

High spin states in ^{34}Cl have been populated by bombarding a 40-MeV ^{12}C beam on an ^{27}Al target at the 14-UD Pelletron accelerator at the Tata Institute of Fundamental Research, Mumbai. The target consisted of 0.50 mg/cm^2 ^{27}Al with 10 mg/cm^2 gold backing to stop the recoils. γ-γ coincidence

*Corresponding author: maitrayee.sahasarkar@saha.ac.in
†Present address: Sidho-Kanho-Birsha University, Purulia 723101, India.

measurement has been done using the multidetector array of 15 Compton-suppressed clover detectors (INGA setup) [10]. The detectors were placed at 157° (3), 140° (2), 115° (2), 90° (4), 65° (2), and 40° (2). A digital data acquisition system based on Pixie-16 modules with 100-MHz sampling rate, developed by XIA LLC [11], has been used. The time-stamped data have been collected in list mode when at least two (Compton-suppressed) clovers were fired in coincidence. The sorting program MARCOS developed at TIFR has been used to generate $E\gamma$-$E\gamma$ matrix. RADWARE [12] and INGASORT [13] programs have been used to analyze the data. A total 6×10^8 γ-γ coincidence data have been recorded during the experiment. Singles data were also collected in the list mode.

Most of the γ rays emitted by the excited states of these light nuclei in this mass region have high energies ($\geqslant$1000 keV). Because long-lived radioactive sources emitting γ rays with energies higher than 1500 keV are not easily available in the laboratory, a radioactive ^{66}Ga($T_{1/2} = 9.41$ h) source has been prepared through ^{56}Fe(^{13}C, $p2n$)^{66}Ga reaction at 50 MeV using the same setup. The energy calibration and the high energy efficiency calibration of the clover detectors have been done using ^{133}Ba, ^{152}Eu, and ^{66}Ga sources.

The experimental data have been sorted into angle-independent and -dependent (90° vs 90°) symmetric γ-γ matrices to build up the level scheme. The multipolarity of the γ-ray transition has been determined from directional correlation of γ rays emitted from excited oriented states (DCO) measurements. The DCO ratio ($R_{\rm DCO}$) [14] of a γ transition (γ_1) is defined as the ratio of intensities of that γ ray (I^{γ_1}) for two different angles in coincidence with another γ ray (γ_2) of known multipolarity. It is given by

$$R_{\rm DCO} = \frac{I^{\gamma_1} \text{ observed at } \theta, \text{ gated by } \gamma_2 \text{ at } 90^\circ}{I^{\gamma_1} \text{ observed at } 90^\circ, \text{ gated by } \gamma_2 \text{ at } \theta}.$$

In our experiment, DCO ratios have been determined for $\theta = 157^\circ$ (Table I). Only in a few cases, to avoid contribution from any contaminant in the area of the γ peak of interest, this ratio has been determined from 65° data (Table I). We have sorted the experimental data into two different angle-dependent asymmetric matrices for DCO measurement. The DCO ratio of each γ has been obtained by putting a gate on a γ transition of known multipolarity with zero or very small mixing ratio. For stretched transition with same multipolarity as the gating transition, $R_{\rm DCO}$ value should be very close to unity. For different multipolarities of the gating and projected transitions, the $R_{\rm DCO}$ value depends on the angle between the detectors and the amount of mixing present in the mixed multipolarity transition. For the assignment of spins and the γ-ray multipole mixing ratios (δ), the experimental DCO values were compared with the theoretical values calculated by using the computer code ANGCOR [14]. Spin alignment parameter $\sigma/J = 0.3$ was used for this calculation.

Clover detectors can be used as polarimeters for measuring the polarization of the γ transitions. We have performed integrated polarization asymmetry measurements (IPDCOs, i.e., integrated polarization –directional correlation from oriented nuclei) [15] to ascertain the electric or magnetic nature of the transitions. Two asymmetric IPDCO matrices were constructed from the data. The first (second) matrix named as parallel (perpendicular) was constructed having on the first axis the simultaneous events recorded in the two crystals of the 90° clover detector which are parallel (perpendicular) to the emission plane and on the second axis the coincident γ ray registered in any other detector. The polarization asymmetry is defined as

$$\Delta_{\rm IPDCO} = \frac{a(E_\gamma)N_\perp - N_\parallel}{a(E_\gamma)N_\perp + N_\parallel}, \quad (1)$$

where $N_\perp$ and $N_\parallel$ are the intensities of the full energy peaks observed in the perpendicular and parallel matrices, respectively. The correction term $a(E_\gamma)$ is introduced owing to asymmetry in the response of the different crystals of the clover detector at 90°. It is defined as

$$a(E_\gamma) = \frac{N_\parallel(\text{unpolarized})}{N_\perp(\text{unpolarized})}. \quad (2)$$

In the present experiment a is measured as a function of energy of unpolarized γ rays from radioactive source ^{152}Eu. This correction term (Fig. 1) has a value close to the unity (Fig. 1) for this setup.

For determination of experimental polarization asymmetry from each of the IPDCO matrices, we have put gates on γ's on the second axis and observed the projected parallel and perpendicular spectra of the 90° clover detectors. A positive (negative) value of $\Delta_{\rm IPDCO}$ indicates a pure electric (magnetic) transition. However, for mixed transitions, usually this value is close to zero and the sign varies depending on the extent of mixing. In Fig. 1, representative projected energy spectra from two different matrices (parallel and perpendicular) of ^{34}Cl have been generated by putting a gate on a 879-keV transition. Comparison of these projected spectra clearly show the electric (magnetic) nature of 491-keV (461-keV) transition. The measured asymmetry is related to the degree of polarization $P(90^\circ)$ by the relation

$$P(90^\circ) = \frac{\Delta_{\rm IPDCO}}{Q}, \quad (3)$$

where Q is the polarization sensitivity of the polarimeter. Q depends on the energy of the γ ray and the geometry of the polarimeter [15]. The theoretical values of $P(90^\circ)$ for each of the transitions have been calculated. The attenuated angular distribution coefficients have been theoretically estimated from Ref. [16] by using the known values of spins, parities of the initial and final states, and the spin alignment factor. The mixing ratios for the transitions are taken from the present work or the literature [4]. The theoretical $P(90^\circ)$ has been then multiplied by $Q(E_\gamma)$ to get the theoretical value of $\Delta_{\rm IPDCO}$. We have determined $Q(E_\gamma)$ for a few stretched quadrupole transitions to get the energy dependence of Q for the present setup (Fig. 2). It agrees well with that obtained for similar setups [17–19].

Lifetime measurements with DSAM have been done using asymmetric matrices having events from a particular angle (157° or 65°) on one axis and the coincidence events from the 90° detectors on the other. Level lifetimes were extracted from the line shape analysis. The modified version of computer code LINESHAPE [20,21], which included corrections for the broad initial recoil momentum distribution produced by the

TABLE I. Relative intensity (I_{rel}), R_{DCO}, Δ_{IPDCO}, and the mixing ratio (δ) of the γ transitions in ^{34}Cl.

E_γ	I_{rel}	J_i	J_f	E_{gate}	ΔJ	R_{DCO}	Mixing ratio (δ)		Δ_{IPDCO}	
(keV)				(keV)			Present	Previous [4]	Exp.	Calc.
453	7.9(1)	3^+	2^+	461	1	1.30(17)	0.11(6)			
461	100(5)	1^+	0^+	491	2	0.49(2)	$M1$		−0.08(1)	−0.20
491	253(1)	7^+	5^+	4678	2	0.99(3)	$E2$		0.14(2)	0.11
563	12.4(2)	2^-	2^+	461	1	1.13(10)	−0.38(6)			
572	21.8(2)	7^+	6^-	879	2	0.44(3)	−0.04(2)	−0.05(2)	0.15(10)	0.05
666	45.0(4)	1^+	0^+	879	2	0.48(4)	$M1$		−0.10(3)	−0.16
725	5.0(2)	4^+	5^+	3500	2	0.38(7)	$M1+E2$		−0.17(12)	
769	19.4(2)	2^+	1^+	461	1	1.13(9)	0.04(3)	1.4(6)		
879	97.5(3)	4^-	2^-	491	2	0.95(5)	$E2$		0.12(2)	0.09
1112	29.5(3)	6^-	5^-	1256	1	1.92(17)	0.36(6)	4.7(6)	−0.03(1)	−0.07
1143	34.4(3)	6^-	4^-	666	1	2.08(18)	$E2$	$E2$	0.07(2)	0.06
1193	8.9(2)	5^+	5^-	1256	1	1.94(36)	−0.1(3)		0.08(2)	0.07
1225	15.5(1)	4^-	4^+	1143	2	1.29(14)	0.3(3)			
1224	34.7(3)	5^+	4^-	879	2	0.42(2)	−0.02(2)	$E1$	0.04(1)	0.03
1256	23.0(2)	5^-	4^+	491	2	0.39(5)	−0.01(4)	0.0(2)	0.010(2)	0.032
1426	8.5(2)	2^+	1^+	461	1	0.71(11)	−0.11(5)	−1.8(2)		
1515	14.5(1)	3^+	1^+	666	1	2.24(20)	$E2$			
1669	13.8(3)	7^+	5^+	1935	2	1.03(38)[a]	$E2$			
1697	22.3(2)	2^+	1^+	461	1	0.74(6)	−0.10(2)	−0.05(3)		
1720	41.3(3)	3^+	1^+	491	2	1.10(16)	$E2$		0.15(6)	0.02
1935	232(3)	9^+	7^+	491	2	1.10(3)	$E2$		0.08(1)	0.03
2035	2.9(1)	3^+	3^+	491	2	0.51(8)	−0.4(1)		0.04(1)	0.03
2055	13.5(2)	2^-	1^+	666	1	0.87(6)	−0.05(3)	>2.5		
2213	2.1(1)	5^+	3^+	491	2	0.69(15)				
2229	40.9(3)	4^+	3^+	491	2	0.90(9)	0.4(1)	6.0(18)	−0.09(3)	−0.03
2260	87.8(5)	2^-	1^+	461	1	1.15(5)	0.05(2)	$E1$	0.04(1)	0.03
2384	18.2(2)	(7^+)	7^+	491	2	0.89(25)[a]			−0.17(11)	
2485	89(1)	8^-	7^+	491	2	0.74(8)	0.22(7)		0.016(2)	0.019
2575	30.2(3)	2^-	3^+	491	2	0.51(12)	−0.3(1)		0.03(1)	0.02
2643	14.7(2)	5^+	3^+	491	2	1.13(13)	$E2$			
2681	3.3(1)	5^-	3^+	461	1	1.88(26)			−0.1(1)	
2721	23.2(2)	2^-	0^+	491	2	0.98(29)	$M2$		−0.06(3)	
2840	47.3(5)	6^+	7^+	491	2	0.83(12)	−0.3(1)		−0.02(1)	−0.01
3381	74(1)	11^+	9^+	491	2	1.00(10)	$E2$		0.03(2)	0.01
3454	85.2(5)	4^-	3^+	491	2	0.68(5)	0.05(5)	0.06(2)	−0.008(1)	0.008
3485	15.4(3)	5^-	3^+	491	2	1.74(47)	−0.23(12)	−0.23(10)	−0.10(4)	
3500	37.2(3)	5^+	3^+	1669	2	0.88(11)	$E2$		0.003(3)	0.011
4077	17.9(5)	9^-	7^+	491	2	1.20(43)	0.2(5)		−0.02(1)	
4597	36.2(3)	6^-	3^+	572	1	3.45(26)		$(E3)$	0.010(2)	
4678	173(3)	5^+	3^+	491	2	1.00(2)	$E2$	$E2$	0.010(1)	0.01

[a]From 65°–90° matrix.

α-particle evaporation, have been used to extract the level lifetime from Doppler shifted spectra. The initial recoil momenta distributions of ^{34}Cl have been obtained from statistical model code PACE4 [22]. In the first step of the LINESHAPE program, the slowing-down histories of the 50 000 ^{34}Cl recoiling nuclei in the ^{27}Al target and Au backing were simulated using the Monte Carlo technique. The velocity profiles of the recoils were generated with a time step of 0.0007 ps. The detector geometry was also taken into account. In the second step, using the stopping powers and the velocity distributions calculated in the first step, a line shape for each decay time was obtained. In the final step, the best fitted theoretically generated line shapes to the experimental ones were obtained by varying the level lifetimes utilizing a χ^2-minimization technique. In this measurement, shell-corrected Northcliffe and Schilling stopping powers [23] were used for calculating the energy loss of ions in matter.

III. RESULTS AND DISCUSSION

A. Level scheme

The level scheme of ^{34}Cl has been extended to $\simeq$10.6 MeV on the basis of coincidence relationship, relative intensities, R_{DCO}, and IPDCO ratios of γ rays. A total projection spectrum as well as typical gated spectra are shown in Fig. 3. γ rays

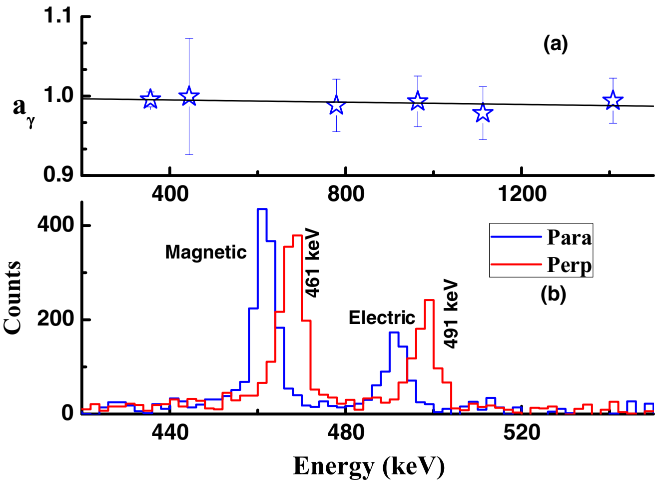

FIG. 1. (Color online) (a) Asymmetry parameter $a(E_\gamma)$ plotted as a function of energy. (b) Spectra generated from perpendicular and parallel matrices indicating the electric (magnetic) nature of the 491-keV (461-keV) transition. The perpendicular spectrum has been artificially shifted for clarity.

from nuclei populated through other dominant channels of the reaction are marked in Fig. 3(a).

From PACE4 calculations, the relative cross section of the ^{27}Al(^{12}C,αn)^{34}Cl channel was predicted as 11.9% of the total fusion. Several new transitions have been identified from the gated spectra generated by putting gates on strong transitions (*viz*., 491, 461, 572, 879 keV, etc.) of ^{34}Cl. We have added 11 new transitions and 6 new levels in the existing level scheme [8] (Fig. 4). Apart from these, 19 transitions and 5 excited levels were observed for the first time in heavy-ion fusion reaction. These transitions were previously observed in light-ion-induced experiments [4].

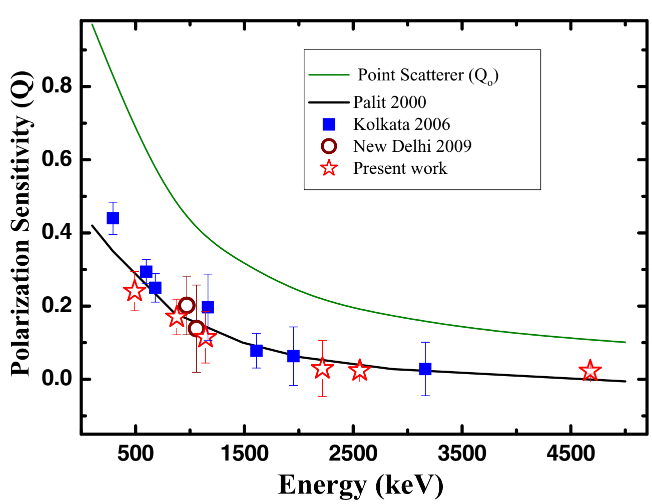

FIG. 2. (Color online) The polarization sensitivity of a clover detector measured as a function of γ energy has been compared with those obtained (i) in a measurement with single clover at similar distance (Palit 2000 [17]) and at different implementations of INGA at (ii) Kolkata (Kolkata 2006 [18]) and (iii) New Delhi (New Delhi 2009 [19]). See text for detail.

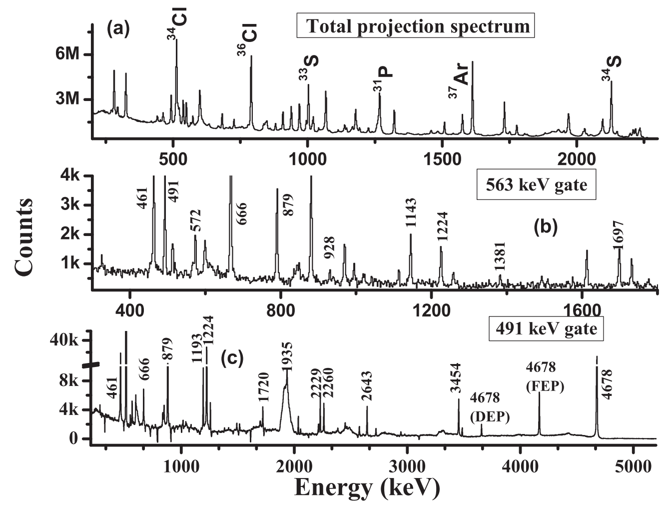

FIG. 3. (a) A total projection spectrum from the present experiment. γ rays emitted by different nuclei populated in the present experiment are marked. Background-subtracted coincidence spectra obtained by putting gates on (b) 563-keV and (c) 491-keV transitions.

Few of these new transitions were totally shifted. To place these transitions in the level scheme, a 90° vs 90° symmetric γ-γ matrix has been used.

To assign the spin and parity of the levels, the conventional DCO and polarization measurements have been performed for most of the γ's. The relative intensities of these transitions have been estimated from 461-keV gated spectrum. For 461 keV and the transitions parallel to 461 keV, relative intensities have been measured from the total projection spectrum and normalized with 879-keV transition. The relative intensities, experimental R_{DCO} values, mixing ratios (for mixed transitions), and experimental and theoretical polarization asymmetry values are listed in Table I. We have calculated the mixing ratios for 20 transitions and compared them with earlier measurements, wherever available (Table I). For a few transitions, *viz*., 769, 1112, 1426, 2055, and 2229 keV, the mixing ratios measured in the present work are significantly lower than those deduced in the past (Table I). We have found that our experimental R_{DCO} values for these transitions can also be reproduced with higher values of mixing ratios (>1) similar to earlier work, indicating their predominant electric nature. However, for two of these transitions (1112 and 2229 keV), our polarization measurements have confirmed their magnetic character. Therefore, we have retained the smaller values of mixing ratios, unlike those deduced earlier. Similarly, for the other three transitions also, we preferred to retain the smaller values of mixing, although the higher values cannot be fully ruled out unless polarization measurements are carried out for them. The experimental R_{DCO} values for few transitions have been plotted with their energies in Fig. 5. Polarization asymmetry (Δ_{IPDCO}) for more than 25 γ transitions in ^{34}Cl have been measured for the first time. The branching ratios of the excited states have been calculated from the present experimental data and compared with the results of earlier measurements (Table II).

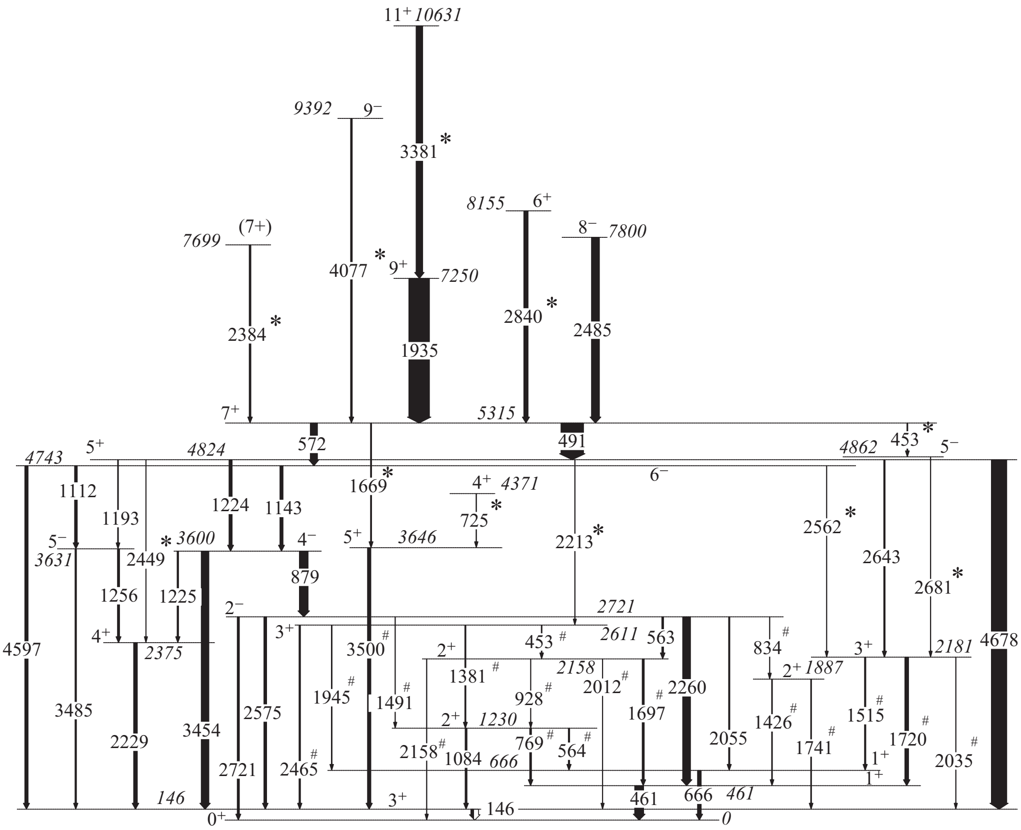

FIG. 4. Partial level scheme of ^{34}Cl. Newly assigned γ transitions and those already observed in light-ion-induced reactions are indicated by $*$ and #, respectively.

1. Levels with excitation energy $\leqslant$3 MeV

At low excitation energy ($\leqslant$3 MeV), four levels (1230, 1887, 2158, and 2611 keV) have been added to the existing level scheme [8]. These levels were already observed in light-ion-induced experiments [4]; however, in a heavy-ion-induced reaction, they are observed for the first time. The spins and parities of these levels have been confirmed from DCO and polarization measurements. From the absolute excitation energy of 2_1^+ state (2127 keV) in $T = 1$ ^{34}S, the 2158 keV state in $T = 0$ ^{34}Cl has been assigned as $T = 1$, $J^\pi = 2^+$ state. In an earlier heavy-ion reaction [8], the 2181-keV level (3_2^+) was shown to be populated by direct feeding transition (2643 keV) without any decay-out transition from this level. However, in light-ion-induced experiments, decay-out transitions (1515, 1720, and 2035 keV) were observed. In the present work also, these decay-out transitions have been observed and their properties have been studied (Table I).

2. Levels with excitation energy between 3 and 6 MeV

Excited levels with excitation energy in between 3 and 6 MeV, which were already observed in light-ion experiments, were also observed in our experiment. These levels and several transitions connecting them have been placed accordingly in the level scheme and their spin-parity assignments were confirmed. Among these states, the 3646-keV level was previously assigned as (3,4,5$^+$) [4]. From $R_{\rm DCO} \simeq 1$ for 3500-keV γ transition emitted from this level for a $\Delta J = 2$ gating transition (Table I) and its positive value of polarization asymmetry, we have confirmed that the spin parity of the 3646-keV level is 5^+. Two new levels, 4371 keV (4^+) and 4862 keV (5^-) and seven new transitions have been added to the existing level scheme [8] in this energy domain.

3. Levels with excitation energy $\geqslant$6 MeV

From the earlier measurements by van der Poel *et al.* [8], owing to low statistics and large Doppler broadening, the spin and parity of the 7250- and 7800-keV levels were assigned as (9^+) and (8^+), respectively. We have eliminated the uncertainty in their spin, parity assignments from DCO, and polarization measurements of the deexciting γ transitions, *viz*., 1935 and 2485 keV from 7250- and 7800-keV levels, respectively (Table I).

A weak and Doppler-broadened γ transition with $E_\gamma = 3381 \pm 2$ keV was previously observed by van der Poel *et al.* [8]. They reported that this transition is in coincidence with the 491-keV transition and, possibly, with a 1935-keV transition. However, owing to low statistics, they could not study its properties in detail. In the present work, we have confirmed that 3381-keV transition is in coincidence with both 491- and 1935-keV transitions and depending on its relative intensity, we have placed this γ just above the 1935-keV transition. Therefore, a new 11^+ level ($E_x = 10\,631$ keV) has been included in the level scheme. Two more Doppler-shifted new magnetic transitions 4077 and 2840 keV in coincidence with

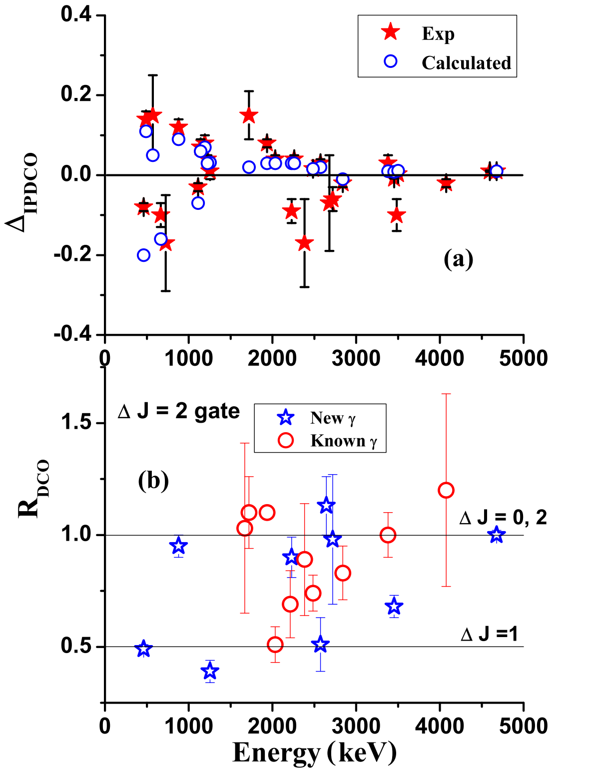

FIG. 5. (Color online) (a) Comparison of experimental and calculated polarization asymmetry (Δ_{IPDCO}) as a function of γ energy. (b) Experimental DCO ratios (R_{DCO}) for few transitions in ^{34}Cl. The two theoretical lines for $\Delta J = 0,2$ and $\Delta J = 1$ have been drawn for mixing ratio $(\delta) = 0$.

491 keV but parallel to 1935 keV were observed. Two new levels at 9392 and 8155 keV have been placed in the level scheme, which are connected through 4077- and 2840-keV γ transitions, respectively, to the 7^+ level at 5315 keV. These two levels (9392 and 8155 keV) have $J^\pi = 9^-$ and 6^+, respectively.

Another weak magnetic Doppler-shifted 2384-keV transition has been placed in the level scheme, which is parallel to 1935 keV but in coincidence with 491 keV. Owing to the large broadening and low statistics, we have large uncertainty in DCO results as shown in Table I. If we compare the position of this level, with 7^+, 8^+, and 9^+ levels in the excitation spectra of ^{36}Cl [24], it seems to be close to the 8_2^+ state in ^{36}Cl. However, from shell-model results (Sec. IV), it was found that the calculated second 7^+ state matches very well with this state, whereas calculated 8^+ state was around 1 MeV above it. In ^{36}Cl also, all these 7^+, 8^+, and 9^+ states were well explained by shell-model calculation [24]. On the basis of these arguments, we have assigned this level at 7699 keV as (7^+).

B. Lifetime measurement

The energy spectra for γ transitions from 7800, 9392, 8155-, and 10 631-keV levels in ^{34}Cl were totally shifted. None of them have any stopped component. These γ's must be emitted in flight and these levels must have the lifetime shorter than the stopping time of the recoils in gold backing. Another

TABLE II. Comparison of experimental and theoretical branching ratios of different excited levels.

Energy (keV)		Branching ratio		
		Exp.		Theor.
Level	γ	Present	Previous [4]	
1230	564	36.4(44)	28(2)	27.2
	769	32.3(44)	38(3)	32.8
	1084	31.3(42)	32(2)	40.0
1887	1426	48.0(35)	59(3)	54.2
	1741	52.0(42)	37(3)	45.8
2158	928	8.6(10)	7(2)	7.6
	1697	62.1(30)	69(4)	62.3
	2012	10.2(10)	7(2)	12.7
	2158	19.1(20)	17(2)	17.4
2181	1515	14.5(17)	13(6)	7.7
	1720	41.4(43)	37(2)	33.5
	2035	44.1(46)	50(2)	58.8
2611	453	19(13)	22(8)	6.8
	1381	28.0(20)	26(2)	33.3
	1945	17.0(13)	16(6)	31.3
	2465	36.0(25)	36(2)	28.6
2721	563	9.8(10)	7(4)	
	834	2.0(2)	2(2)	
	1491	2.1(2)	2(2)	
	2055	7.5(8)	8(4)	
	2260	48.9(48)	47(7)	
	2575	16.8(17)	18(4)	
	2721	12.9(13)	16(6)	
3600	879	49.2(18)	51(2)	
	1225	7.8(4)	7(2)	
	3454	43.0(18)	42(2)	
3631	1256	52.5(13)	60(2)	
	3485	47.5(13)	40(2)	
4743	1112	29.2(28)	31(2)	
	1143	34.0(33)	37(2)	
	2562	1.0(1)		
	4597	35.8(36)	32(2)	
4824	1193	5.1(1)	4(1)	
	1224	14.8(1)	19(2)	
	2213	1.6(1)		
	2449	1.5(1)		
	2643	4.8(6)	7(1)	
	4678	72.2(2)	70(2)	
5315	453	2.8(1)		
	491	72.2(3)	74(1)	
	572	21.6(2)	26(1)	
	1669	3.5(2)		

transition emitted from the 7250-keV level was not fully shifted but had a large Doppler-shifted component along with a stopped component. In the present work, we have extracted the lifetimes of these levels from line-shape analysis. Usually in line-shape analysis, the angle-dependent line-shape spectra are generated by putting a gate above the transition of interest to remove the side feeding effect. However, owing to the low population yields of higher energy levels, generation of gated spectra using a transition above the transition of interest was

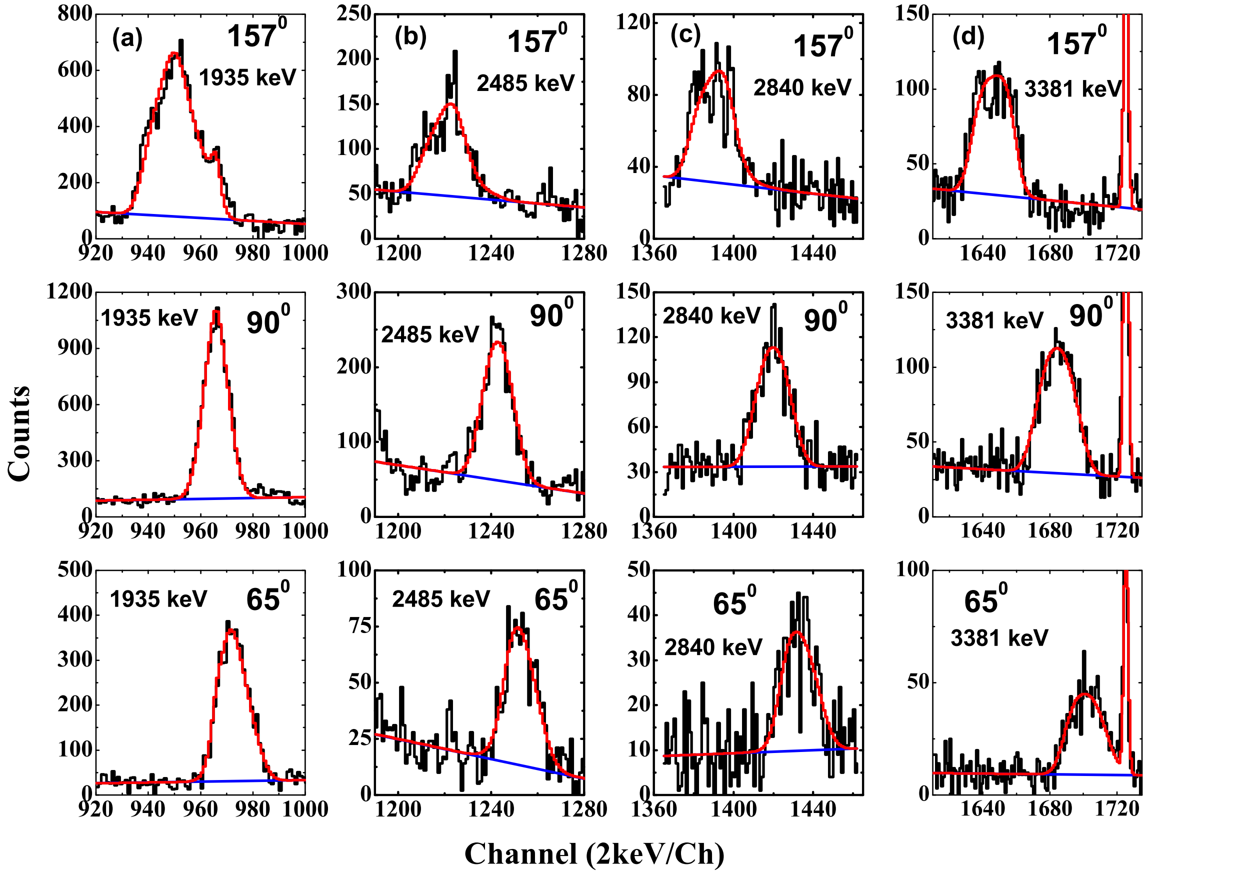

FIG. 6. (Color online) Experimental (black) and simulated (red) line-shape spectra are shown for (a) 1935-keV (b) 2485-keV, (c) 2840-keV, and (d) 3381-keV transitions for different angles as marked in the figure.

not possible in the present data. Therefore, the level lifetimes have been extracted using spectra generated by putting gates on transitions below the Doppler-shifted transition (GTB). Hence, for each level we have to consider the side feeding effect with proper care.

The mean life of 7250-keV level (200 ± 70 fs) has been reported by van der Poel *et al*. with large uncertainty owing to their thick target experiment [8]. In the present work, we have remeasured (Table V) the lifetime of this level from GTB spectra of 1935-keV transition for three different angles by putting a gate on the 491-keV transition (Fig. 6). The side feeding effects have been considered very carefully. We have fitted the experimental spectra of 3381- and 1935-keV transitions simultaneously as members of a single band. The rotational cascade side feeding with five transitions has been considered, assuming 100% feeding to the topmost level of the band. So we could only set the upper limit of the mean life of the 10 631-keV level. Similarly, for 7699-, 7800-, 8155-, and 9392-keV levels (Fig. 7) also, upper limits to their lifetimes have been obtained, as no feeding transitions to these levels have been observed in the present work (Table V).

Coexistence of deformed or superdeformed states along with those generated from single-particle excitations has generated new interest in this mass region [1]. In a recent work, a negative-parity band has been observed in ^{35}Cl [1], which evolves from single-particle excitation ($\simeq$5 W.u.) at low spins to collectivity and superdeformation ($\simeq$20–33 W.u.) at high spins. In ^{34}Cl, we have calculated the reduced transition probabilities from the lifetimes. We have found that for $E2$ transitions, the $B(E2)$ values lie within 8–20 W.u., indicating

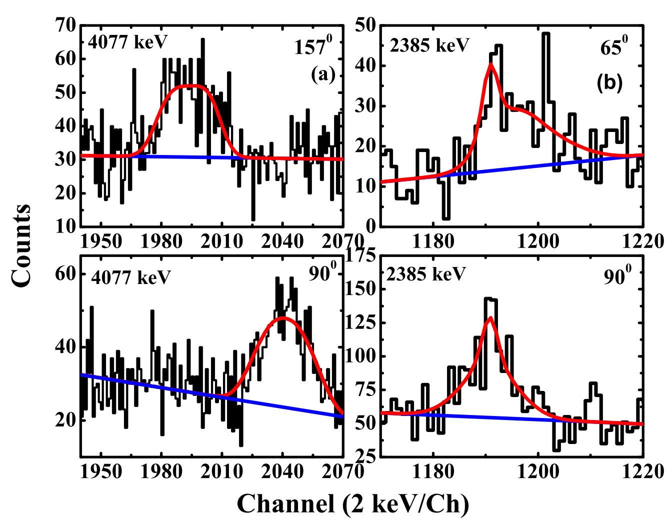

FIG. 7. (Color online) Experimental (black) and simulated (red) line-shape spectra are shown for (a) 4077-keV and (b) 2384-keV transitions for different angles as indicated in the figure.

the presence of collectivity at higher excitation energy. The corresponding deformation parameter β_2 and the extracted major to minor ratio X [25] clearly show that 10.631-MeV (11^+), 7.250-MeV (9^+) and 5.315-MeV (7^+) states which were connected by $E2$ transitions (3381 and 1935 keV, respectively) form a deformed band having deformation $\beta_2 \simeq 0.19$–0.29. The major to minor ratios X of the spheroids corresponding to these deformations are 1.20 and 1.32, respectively. These results give a clear indication of collective excitation in ^{34}Cl above 5-MeV excitation energy.

IV. THEORETICAL CALCULATION

Large-basis shell-model calculations have been done using the code OXBASH [26] to learn about the microscopic origin of each excited state in ^{34}Cl. The valence space consists of both sd-pf shells with $1d_{5/2}$, $1d_{3/2}$, $2s_{1/2}$, $1f_{7/2}$, $1f_{5/2}$, $2p_{3/2}$, and $2p_{1/2}$ orbitals for both protons and neutrons above the ^{16}O inert core. ^{34}Cl is a self-conjugate nucleus and the number of valence particles (protons + neutrons) in ^{34}Cl is 18. The *sdpfmw* interaction [27] (as referred to within the OXBASH code package) was used for the calculation. Other relevant details of the interaction and calculation are discussed in Ref. [5].

Unrestricted calculations for nuclei having such a large number of valence particles in the full valence space often led to a prohibitively large m-scheme basis dimension. Several truncation methods have therefore been used for shell-model studies of these nuclei. Different truncation schemes and corresponding results for energy spectra and transition probabilities are discussed in the next sections. For all these calculations, the mass normalization factor for the sd shell interaction was taken accordingly, depending on the number of particles in the sd shell; e.g., for Theo-P1 it was 34 and for the other two truncations Theo-P2 and Theo-P3, it was 32. These results obtained with different truncation schemes helped us to understand the effect of extending the inert core from ^{16}O to ^{28}Si by using completely filled $1d_{5/2}$ orbital in the calculations. They also clearly indicated the minimum number of nucleons

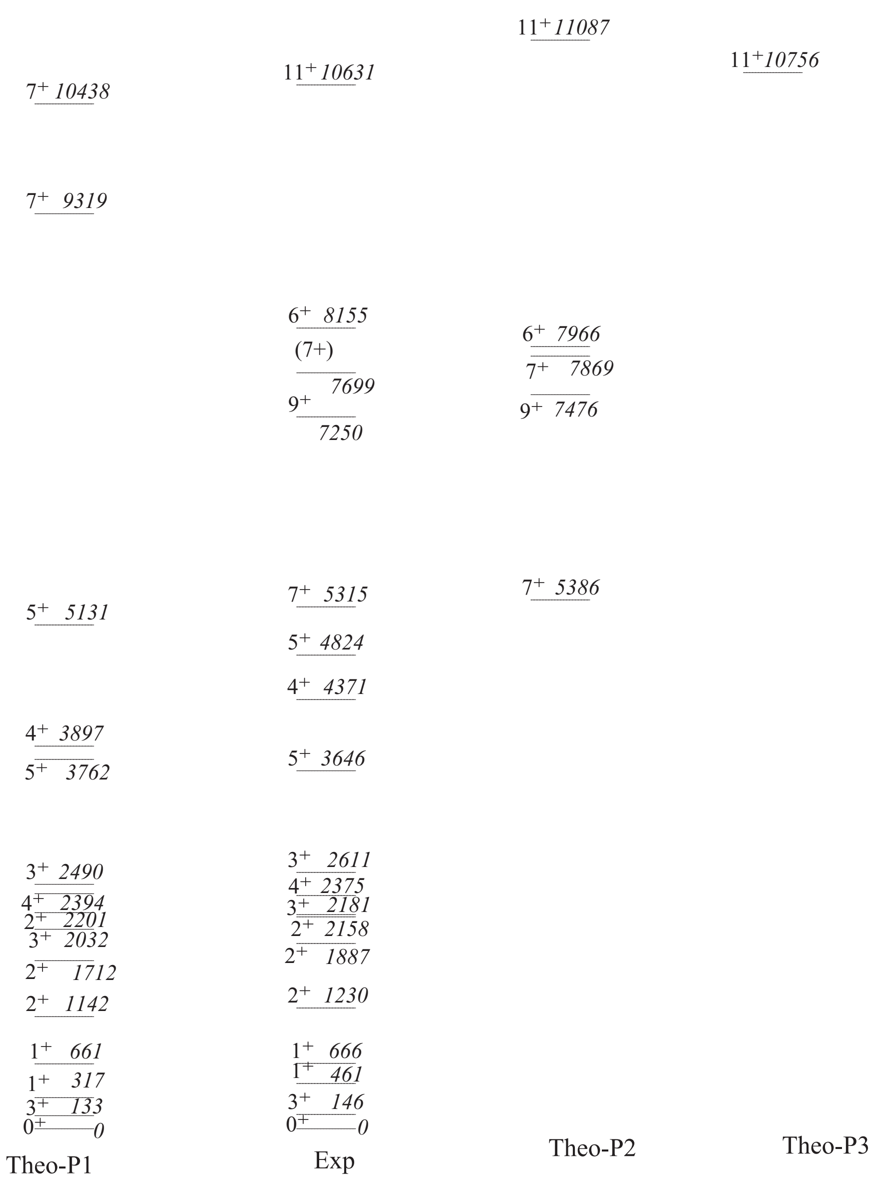

FIG. 8. Comparison of theoretical and experimental level schemes for positive-parity states in ^{34}Cl for different truncation schemes as discussed in the text. All these energies are plotted considering the ground-state energy (−202.652 MeV) as 0.

needed in the pf shell to reproduce the experimental data for any particular state.

In the level scheme, several $E1$ transitions have been observed. However, we were not able to calculate the theoretical branching ratios for the levels having $E1$ decay-out transitions. These calculated values vanish owing to the isospin selection rule [28], which states that $E1$ transition in self-conjugate nuclei (^{34}Cl, $N = Z = 17$) for $\Delta T = 0$ is forbidden. The nonzero strengths of experimental $B(E1)$ values are therefore interesting and may be utilized to determine the extent of isospin mixing prevailing in this nucleus [29].

A. Positive-parity states

We have used three different truncation schemes named Theo-P1, Theo-P2, and Theo-P3 to reproduce the positive-parity states in ^{34}Cl (Fig. 8).

1. Truncation scheme Theo-P1

In Theo-P1, only $0\hbar\omega$ excitation was considered; i.e., only the full sd shell was the model space. The calculated ground-state binding energy of ^{34}Cl is −202.652 MeV, which agrees well with the experimental binding energy −202.681 MeV (corrected for Coulomb energy) [30]. The maximum possible spin which can be generated in full sd model space for ^{34}Cl is 11^+. In this truncation (Theo-P1), the calculated excitation spectra matches well with the experimental level scheme up to 5^+ angular momentum states. For higher spins, the calculated energy values are overpredicted by several MeV, indicating the need for inclusion of contribution from the neighboring pf orbitals.

2. Truncation scheme Theo-P3

Hence, in Theo-P3, we have included all the pf orbitals in our calculations where only two particles are allowed to be excited in the pf shell. However, owing to the computational limitation, only the 11^+ state could be calculated and the calculated absolute energy has good agreement with the experimental data (shown as Theo-P3 in Fig. 8).

3. Truncation scheme Theo-P2

In Theo-P2, the $1d_{5/2}$ orbital has been completely filled up and made inert to overcome the dimensionality problem. This truncation also leads to overprediction of level energies. However, the relative spacing between two consecutive states (say spacing between 9_1^+ and 7_1^+ states) are reproduced well. So in the next step, similar to our earlier work [1,5], we have reduced the single-particle energy (SPE) of pf orbitals by 4.35 MeV to reproduce the absolute energy (−197.366 MeV) of 7^+ states. This depression improves the calculated energies and they match very well with the experimental energies. Only the energy of the 11_1^+ state has been overpredicted by 0.5 MeV, showing the need for making the $1d_{5/2}$ orbital active.

B. Negative-parity states

Similarly for negative-parity states, different truncation schemes have been adopted (Fig. 10).

1. Truncation scheme Theo-N1

In Theo-N1, we have considered 1p-1h excitation, i.e., excited one nucleon into the pf shell to reproduce the negative-parity states. The mass normalization factor for sd shell two-body matrix elements (TBMEs) for this calculation was taken to be 33. In this scheme, the first three negative-parity states (2^-, 4^-, and 5^-) were underpredicted, whereas 6^-, 8^-, and 9^- states were overpredicted. Apart from these, the positions of the first 5^- and 4^- states have also been interchanged in the theoretical results.

2. Truncation scheme Theo-N2

It is well known that overpredicted energies indicate inadequacy of the model space. Results can be improved by either including more orbitals in the model space or by increasing the contribution from pf orbitals by exciting more particles in them. However, if the calculated spectra are underpredicted compared to experimental data, we can improve it by taking measures to reduce the extent of configuration mixing in

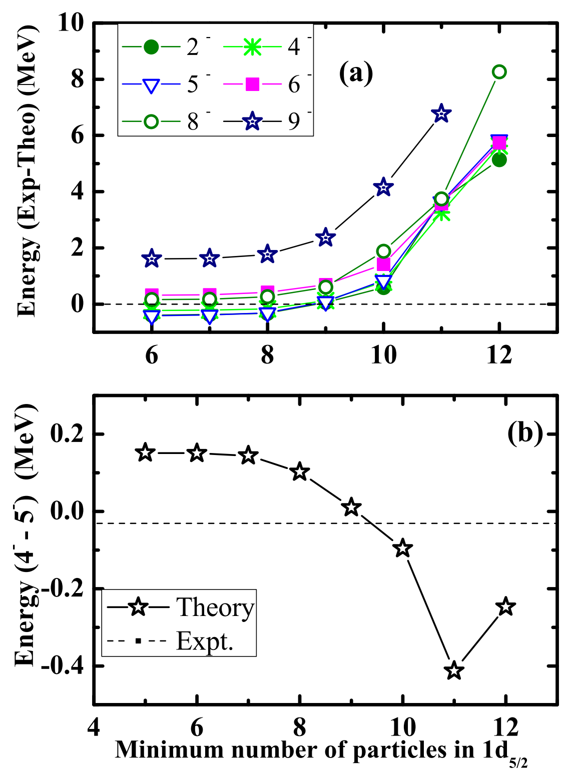

FIG. 9. (Color online) (a) Variations of theoretical predictions compared to experimental energies of different spin states are shown as functions of particle number restriction in the $1d_{5/2}$ orbital. (b) Theoretical energy difference between 4^- and 5^- states for different particle number restriction in the $1d_{5/2}$ orbital. The dotted line indicates the experimentally observed energy spacing between these levels.

the wave functions. We can improve the results by either increasing the mass normalization constant from 33 or by decreasing the SPEs of pf orbitals. However, we preferred to work using a different approach. We have used new truncation schemes by restricting the number of particles in $1d_{5/2}$ orbital (Theo-N2). It is found (Fig. 9) that for the first three negative-parity states, the calculated energies match very well with theory for Theo-N2 [$(1d_{5/2})^{9-12}$ $(2s_{1/2}1d_{3/2})^{5-8}(pf)^1$ particle partition]. Although in Theo-N2, the 5^- state still appeared above the 4^- state, the relative spacing between these states has been reduced to 10 keV from 151 keV in Theo-N1. The relative spacings between 4^- and 5^- states have been plotted in Fig. 9 for different particle restrictions in $1d_{5/2}$ orbital. For 6^-, 8^-, and 9^- states, the overpredicted energies with $(1d_{5/2})^{9-12}(2s_{1/2}1d_{3/2})^{5-8}$ $(pf)^1$ particle partition indicates that we need other partitions for these states. These states were also overpredicted for the full sd-pf model space calculation with $1\hbar\omega$ excitation (Theo-N1). It is therefore evident that more particles need to be excited to the pf shell to reproduce these states.

3. Truncation scheme Theo-N3

For high spin negative-parity states (6^-, 8^-, and 9^-), we have included both one- and three-particle excitations to the pf shell in our calculation (Theo-N3). In this scheme, the full sd-pf space has been used for 1p-1h excitation. However, owing to computational limitation, the $1d_{5/2}$ orbital has been kept completely filled with 12 particles for 3p-3h excitation. The SPE values for pf orbitals and the mass normalization factor remain unchanged (same as in Theo-N2) for this truncation. We found (Fig. 10) that the 6^-, and 8^- states have been reproduced well, but still the 9^- state was overpredicted by 1.6 MeV. The relative percentages of 3p-3h mixing in 6^- and 8^- states were 5% and 0.5%, respectively.

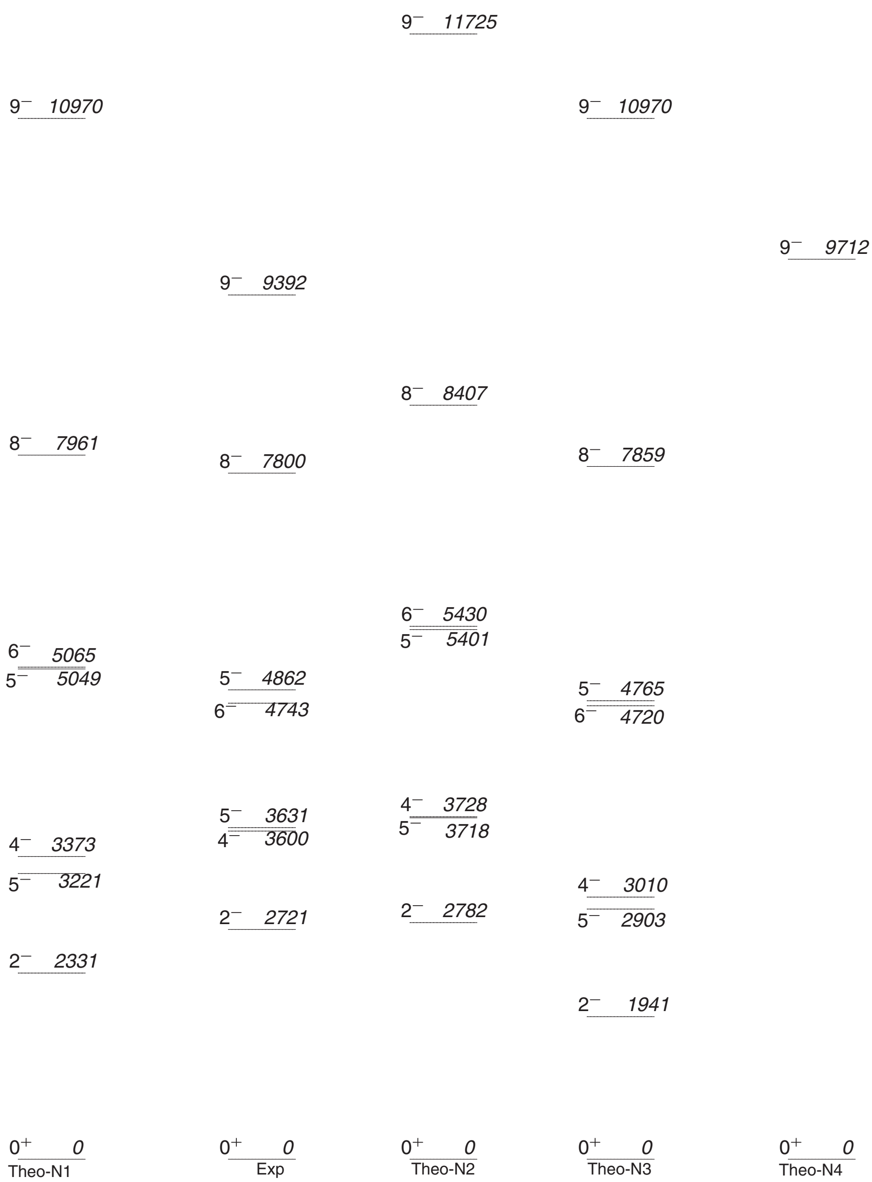

FIG. 10. Comparison of theoretical and experimental level schemes for negative-parity states in ^{34}Cl for different truncation schemes as discussed in the text. All these energies are plotted considering the ground state energy (−202.652 MeV) as 0.

4. Truncation scheme Theo-N4

To reproduce the 9^- state, pure 3p-3h ($3\hbar\omega$) excitation has been considered (Theo-N4). In Theo-N4, the $1d_{5/2}$ orbital was kept inert and the SPE of pf orbitals were suppressed by the same amount (4.35 MeV) as used in Theo-P3. The mass normalization factor for sd-shell TBMEs has been taken as 31 for $3\hbar\omega$ excitation. The results show good agreement between experimental and calculated 9^- state energy values. Therefore, we understand that pure 3p-3h excitation with proper renormalization of the sd-pf shell gap is important to reproduce the 9^- state.

TABLE III. Structure of the wave functions for full sd shell calculation. The partitions are given in terms of particle numbers in single-particle valence states in the following order $1d_{5/2}$, $1d_{3/2}$ and $2s_{1/2}$. See text for detail.

J_i^π	T	Energy (MeV)		Wave function		N_1	N_2
		Exp.	Theor.	(%)	Partition		
0_1^+	1	0 (−202.681)	0 (−202.652)	48	[12,2,4]	11	2
				18	[10,4,4]		
				15	[12,4,2]		
3_1^+	0	0.146	0.133	52	[12,2,4]	9	4
				16	[10,4,4]		
				10	[12,4,2]		
1_1^+	0	0.461	0.317	32	[12,3,3]	12	3
				17	[12,4,2]		
				11	[10,5,3]		
1_2^+	0	0.666	0.661	38	[12,2,4]	11	2
				18	[12,3,3]		
				10	[11,4,3]		
				10	[10,4,4]		
2_1^+	0	1.230	1.142	48	[12,3,3]	10	2
				10	[12,4,2]		
				10	[10,5,3]		
				10	[11,4,3]		
2_2^+	0	1.887	1.712	33	[12,4,2]	12	1
				12	[12,5,1]		
				12	[11,4,3]		
				10	[12,3,3]		
2_1^+	1	2.158	2.201	25	[12,2,4]	12	3
				25	[12,3,3]		
				11	[11,4,3]		
3_2^+	0	2.181	2.032	28	[12,3,3]	13	3
				13	[11,4,3]		
				11	[12,5,1]		
				10	[10,5,3]		
4_1^+	0	2.375	2.394	44	[12,3,3]	11	2
				18	[11,4,3]		
				10	[10,5,3]		
				10	[12,5,1]		
3_3^+	0	2.611	2.490	21	[12,4,2]	12	2
				16	[11,3,4]		
				15	[12,3,3]		
				12	[11,5,2]		
				10	[11,4,3]		
5_1^+	0	3.646	3.762	49	[11,3,4]	8	2
				20	[12,4,2]		
				10	[11,5,2]		
4_2^+	0	4.371	3.897	22	[11,4,3]	12	1
				17	[12,5,1]		
				17	[12,4,2]		
5_2^+	0	4.824	5.131	27	[11,4,3]	9	3
				27	[10,4,4]		
				15	[11,5,2]		

C. Configuration mixing and collectivity

The decompositions of the wave functions are shown in the Tables III and IV. Results from Theo-P1 and Theo-P3 are tabulated for the 0^+ to 5^+ states and the 11^+ state, respectively. For the remaining positive-parity states, results are from Theo-

TABLE IV. Structure of the wave functions in (sd-pf) space. The partitions are given in terms of particle numbers in single-particle valence states in the following order: $1d_{5/2}$, $1d_{3/2}$, $2s_{1/2}$, $1f_{7/2}$, $1f_{5/2}$, $2p_{3/2}$, $2p_{1/2}$. See text for detail.

J_i^π	T	Energy (MeV)		Wave function		N_1	N_2
		Exp.	Theor.	(%)	Partition		
2_1^-	0	2.721	2.331	42	[12,1,4,1,0,0,0]	14	7
				15	[10,3,4,1,0,0,0]		
				11	[12,3,2,1,0,0,0]		
4_1^-	0	3.600	3.373	39	[12,2,3,1,0,0,0]	13	8
				12	[10,4,3,1,0,0,0]		
5_1^-	0	3.631	3.221	33	[12,1,4,1,0,0,0]	16	6
				13	[10,3,4,1,0,0,0]		
				11	[12,3,2,1,0,0,0]		
6_1^-	0	4.743	4.720	28	[12,2,3,1,0,0,0]	13	12
				12	[12,3,2,1,0,0,0]		
5_2^-	0	4.862	5.049	23	[12,2,3,1,0,0,0]	15	9
				11	[12,4,1,1,0,0,0]		
				11	[11,3,3,1,0,0,0]		
7_1^+	0	5.315	5.386	31	[12,0,4,2,0,0,0]	8	3
				28	[12,2,2,2,0,0,0]		
				10	[12,1,3,1,0,1,0]		
9_1^+	0	7.250	7.476	42	[12,1,3,2,0,0,0]	6	1
				26	[12,3,1,2,0,0,0]		
				17	[12,2,2,2,0,0,0]		
7_2^+	0	7.699	7.869	34	[12,0,4,2,0,0,0]	6	5
				31	[12,4,0,2,0,0,0]		
				10	[12,2,2,2,0,0,0]		
				10	[12,1,3,2,0,0,0]		
8_1^-	0	7.800	7.859	28	[11,2,4,1,0,0,0]	12	7
				23	[12,3,2,1,0,0,0]		
				12	[11,4,2,1,0,0,0]		
6_1^+	1	8.155	7.966	27	[12,2,2,1,1,0,0]	10	5
				24	[12,0,4,2,0,0,0]		
				12	[12,1,3,2,0,0,0]		
9_1^-	0	9.392	9.862	31	[12,2,1,3,0,0,0]	8	7
				20	[12,3,0,3,0,0,0]		
				15	[12,1,2,3,0,0,0]		
				12	[12,0,3,3,0,0,0]		
11_1^+	0	10.618	10.756	19	[12,2,2,2,0,0,0]	17	8
				12	[11,3,2,2,0,0,0]		
				10	[12,3,1,2,0,0,0]		

TABLE V. Comparison of experimental and theoretical reduced transition probabilities for different transitions in ^{34}Cl.

E_X	τ_{mean}(ps)		J_i^π	E_γ	J_f^π	$B(M1)$ ($\times 10^{-2}\mu_N^2$)		$B(M2)$ (μ_N^2 fm^2)		$B(E2)$ (e^2 fm^4)	
(keV)	Reported [4]	Present work		(keV)		Exp.	Theor.	Exp.	Theor.	Exp.	Theor.
461	7.5(6)	—	1_1^+	461	0_1^+	7.61(70)	10.90				
666	13.3(6)	—	1_2^+	666	0_1^+	1.43(9)	1.80				
1230	19.6(13)	—	2_1^+	564	1_2^+	0.58(8)	0.72				
			2_1^+	769	1_1^+	0.20(3)	0.25				
1887	1.7(7)	—	2_2^+	1426	1_1^+	0.53(22)	0.23				
2158	0.0478(32)	—	2_3^+	1697	1_1^+	15(10)	12				
			2_3^+	2158	0_1^+					68(5)	52
2181	0.503(73)	—	3_2^+	1515	1_2^+					29(5)	14
			3_2^+	1720	1_1^+					44(8)	32
			3_2^+	2035	3_1^+	0.50(9)	0.05				
2375	0.216(24)	—	4_1^+	2229	3_1^+	0.20(3)	0.14				
2611	0.231(55)	—	3_3^+	453	2_1^+	49(14)	5.5				
			3_3^+	1945	1_2^+					21(5)	12
2721	>2.0	—	2_1^-	2721	0_1^+			<31.0(35)	30.1		
3600	23(6)	—	4_1^-	879	2_1^-					33(8)	31
3631	280(61)	—	5_1^-	3485	3_1^+			0.23(5)	0.13		
3646	0.22(9)	—	5_1^+	3500	3_1^+					7.2(26)	9.8
4743	7.1(30)	—	6_1^-	1112	5_1^-	0.15(7)	0.03				
			6_1^-	1143	4_1^-					20(8)	6.4
7250	0.202(72)	0.23(4)	9_1^+	1935	7_1^+					130(29)	102
7699	—	<0.49	(7_2^+)	2384	7_1^+	>0.84	—				
7800	0.101(72)	<0.12	8_1^-	2485	7_1^+					$>3.30\times10^{-4}$[a]	
8155	—	<0.08	6_1^+	2840	7_1^+	2.78(65)	0.34				
9392	—	<0.01	9_1^-	4077	7_1^+			>6504	0.19		
10 631	—	<0.04	11_1^+	3381	9_1^+					>51	39

[a] $B(E1)$ in e^2 fm^2.

P2. Similarly for negative-parity states, Theo-N2, Theo-N3, and Theo-N4 have been considered for (2^-, 4^-, 5^-), (6^-, 8^-), and 9^- states, respectively. A general particle partition is given by ($j_1^{m_1} \otimes j_2^{m_1} \otimes \cdots \otimes j_n^{m_n}$), where $m_1 + m_2 + \cdots + m_n = m$, m being the total number of valence particles. A particle partition includes many different configurations owing to various intermediate coupling of angular momenta and isospins. The probability and the structure (i.e., m_1,m_2, ... ,m_n) of various partitions with >10% contribution are shown in the table. The partitions are given in terms of occupation numbers of single-particle valence states. N_1 is the total number of particle partitions for a particular state, each with contribution >1%. The other number N_2 gives an estimation of the minimum number of particle partitions, each of which contribute $\leqslant$1% in the state.

We have already discussed deformation at high spin states in ^{34}Cl. Large experimental $B(E2)$ values (Table V) and configuration mixing obtained from shell-model calculations confirmed the existence of deformed states at higher excitation energies. Most of the positive-parity states show substantial configuration mixing. It is found (Tables III and IV) that 10–17 particle partitions contribute at least 1% in their wave functions. The largest contribution from a single partition ranges from 19% to 52%. These wave functions can be compared with those [5] for the positive-parity states in ^{35}Cl which is only one nucleon away from the self-conjugate ^{34}Cl. The yrast positive-parity states in ^{35}Cl have a much smaller extent of configuration mixing with the largest contribution from a single partition in the range 40%–70%. Negative-parity states in ^{34}Cl also have have similar wave-function structure. Twelve to 16 particle partitions with largest contribution ranging from 23%–42% are observed for these states.

The experimental reduced transition probabilities for transitions with different multipolarities in ^{34}Cl, have been calculated using the standard relations between B(L) and the level lifetimes obtained from the present work or earlier literature [4]. The results for transition probabilities (Table V) also show remarkably good agreement in most of the cases, providing strong evidence in favor of the reliability of the calculated wave functions. In this calculation, the effective charges $e_p = 1.5e$ and $e_n = 0.5e$ and the free values of g factors have been used. It can be seen that at low spin also, the $B(E2)$ values were relatively larger than the single-particle estimates. This type of collective structure at low spin states has already been observed for the positive-parity states in self-conjugate ^{30}P [31] ($N = Z = 15$) in the mid-sd shell.

V. CONCLUSION

High spin states of ^{34}Cl have been studied using the heavy-ion reaction ^{27}Al(^{12}C,αn)^{34}Cl. We have extended the level scheme by adding 11 new transitions and 6 new levels. Apart from these, 19 γ transitions and 5 levels which were already observed in light-ion-induced experiments have been identified. The DCO and polarization measurements have been done to assign the spin and parity of the levels. For the first time we have measured the IPDCO ratios for more than 25 γ transitions, which compare quite well with the calculated values. The branching ratios have also been measured for more than 15 levels and compared with earlier measurements as well as with shell-model results. The lifetimes of six levels have been determined by using line-shape analysis. We have identified a few deformed states at high excitation energy in ^{34}Cl. The LBSM calculations for different truncation schemes have been done to understand the microscopic origin of each level in this self-conjugate nucleus. All the positive- and negative-parity states are reproduced reliably in theoretical calculations. The reduced transition probabilities for some transitions were also calculated and compared with the experimental values. The results obtained with different truncation schemes were important to delineate the effects of changing the inert core from ^{16}O to ^{28}Si and of different particle-number restrictions in the pf shell to reproduce the experimental data for any particular state.

ACKNOWLEDGMENTS

The authors sincerely thank P. K. Das (SINP), S. K. Jadhav (TIFR), and P. B. Chavan (TIFR) for their technical help before and during the experiment. Thanks are due to the target laboratory of VECC, Kolkata, for preparation of the target. Special thanks are due to the Pelletron staff for nearly uninterrupted beam. One of the authors (A.B.) has been financially supported by Council of Scientific and Industrial Research (CSIR), India, under Contract No. 09/489(0068)/2009-EMR-1.

[1] A. Bisoi *et al.*, Phys. Rev. C **88**, 034303 (2013)
[2] C. E. Svensson *et al.*, Phys. Rev. Lett. **85**, 2693 (2000); Phys. Rev. C **63**, 061301(R) (2001).
[3] E. Ideguchi *et al.*, Phys. Rev. Lett. **87**, 222501 (2001); C. J. Chiara *et al.*, Phys. Rev. C **67**, 041303(R) (2003).
[4] http://www.nndc.bnl.gov.
[5] R. Kshetri *et al.*, Nucl. Phys. A **781**, 277 (2007).
[6] B. A. Brown and W. A. Richter, Phys. Rev. C **74**, 034315 (2006).
[7] A. Coc, M. G. Porquet, and F. Nowacki, Phys. Rev. C **61**, 015801 (1999); B. M. Freeman, C. Wrede, B. G. Delbridge, A. Garcia, A. Knecht, A. Parikh, and A. L. Sallaska, *ibid.* **83**, 048801 (2011).
[8] C. J. van der Poel *et al.*, Nucl. Phys. A **373**, 81 (1982).
[9] P. Baumann, A. M. Bergdolt, G. Bergdolt, A. Huck, G. Walter, H. Fromm, and H. V. Klapdor, Phys. Rev. C **18**, 247 (1978); P. Baumann, A. M. Bergdolt, G. Bergdolt, A. Huck, and G. Walter, *ibid.* **18**, 2470 (1978).
[10] R. Palit, Proc. DAE-BRNS Symp. Nucl. Phys. (India) **55**, I11 (2010), http://www.sympnp.org/proceedings/.
[11] H. Tan *et al.*, *Nuclear Science Symposium Conference Record 2008* (IEEE, Washington, DC, 2008), p. 3196.
[12] D. C. Radford, Nucl. Instrum. Methods A **361**, 297 (1995).
[13] R. Bhowmick *et al.*, Proc. DAE-BRNS Symp. Nucl. Phys. (India) B **44**, 422 (2010), http://www.sympnp.org/proceedings/.
[14] E. S. Macias, W. D. Ruhter, D. C. Camp, and R. G. Lanier, Comput. Phys. Commun. **11**, 75 (1976).
[15] K. Starosta *et al.*, Nucl. Instrum. Methods A **423**, 16 (1999).
[16] E. D. Mateosian *et al.*, At. Data Nucl. Data Tables **13**, 391 (1974).
[17] R. Palit *et al.*, Pramana **54**, 347 (2000); M. Saha Sarkar, A. Bisoi, S. Ray, R. Kshetri, and S. Sarkar, arXiv:1308.0207v2 [nucl-ex].
[18] R. Raut *et al.*, Proc. DAE-BRNS Symp. Nucl. Phys. B **47**, 578 (2004), http://www.sympnp.org/proceedings/.
[19] S. Muralithar *et al.*, Nucl. Instrum. Methods A **622**, 281 (2010).
[20] J. C. Wells and N. R. Johnson, Report ORNL-6689, 1991, p.44.
[21] R. K. Bhowmik (private communication).
[22] A. Gavron, Phys. Rev. C **21**, 230 (1980).
[23] L. C. Northcliffe and R. F. Schilling, Nucl. Data Tables **A7**, 233 (1970).
[24] S. Aydin *et al.*, Phys. Rev. C **86**, 024320 (2012).
[25] http://www.physics.mcmaster.ca/~balraj/sdbook/.
[26] B. A. Brown, A. Etchegoyen, W. D. M. Rae, and N. S. Godwin, MSU-NSCL Report No. 524, 1985.
[27] E. K. Warburton, J. A. Becker, and B. A. Brown, Phys. Rev. C **41**, 1147 (1990).
[28] E. K. Warburton and J. Weneser, *Isospin in Nuclear Physics* (North-Holland, Amsterdam, 1969), p. 174.
[29] E. Farnea *et al.*, Phys. Lett. B **551**, 56 (2003); A. Bisoi, M. Saha Sarkar, and S. Sarkar (unpublished).
[30] G. Audi, A. H. Wapstra, and C. Thibault, Nucl. Phys. A **729**, 337 (2003); B. J. Cole, J. Phys. G: Nucl. Phys. **11**, 351 (1985).
[31] I. Ray *et al.*, Phys. Rev. C **76**, 034315 (2007).